High-Temperature Air and Steam Oxidation of XM-19 for SMR Applications: Grain Size Effect and Comparison with 304 Stainless Steel

*Seungyoon Baik[a], Hyung-Ha Jin[b], Chansun Shin[*a]*
[a]*Department of Materials Science and Engineering, Myongji University, Yongin 17058, Republic of Korea*
[b]*Korea Atomic Energy Research Institute, Daejeon 34057, Republic of Korea*

[*]*Corresponding author: c.shin@mju.ac.kr*

***Keywords: SMR, XM-19, 304, High-temperature oxidation, Grain size**

1. Introduction

The increasing demand for carbon-neutral energy has renewed interest in advanced nuclear systems, including small modular reactors (SMRs), which require structural materials that can sustain integrity under high-temperature, oxidizing, and steam-containing environments. In particular, oxidation in steam is often more aggressive than in dry air because water vapor can accelerate oxide growth and promote degradation of protective scales through cracking, spallation, and associated transitions to less protective Fe-rich oxides. Despite extensive studies on the high-temperature oxidation of conventional austenitic stainless steels, quantitative datasets for many candidate alloys under steam-rich conditions remain comparatively limited.

XM-19 (Nitronic 50) is a nitrogen-strengthened austenitic stainless steel that offers higher mechanical strength and good corrosion resistance relative to conventional 300-series alloys (e.g., type 304), making it a potential candidate for demanding nuclear-service components. However, its high-temperature oxidation behavior in steam, including the stability of oxide-scale architectures and the propensity for breakaway-type kinetics, has not been systematically established across accident-relevant temperature ranges. In addition, microstructural factors such as grain size can influence oxidation kinetics and scale morphology by modifying diffusion pathways (e.g., along grain boundaries) and affecting the nucleation and continuity of Cr-rich protective layers.

In this study, the high-temperature oxidation behavior of XM-19 is investigated in comparison with type 304 stainless steel in air and steam over 800–1100 ℃, with emphasis on the grain-size effect. Oxidation kinetics and oxide-scale evolution are evaluated using continuous weight-gain measurements, phase identification by X-ray diffraction (XRD), and microstructural/chemical characterization of oxide scales.

2. Experimental

XM-19 specimens with dimensions of 20 mm × 8 mm × 3.5 mm were used for oxidation testing. To suspend the specimen from the microbalance, a hole was drilled at the top of each specimen. The alloy composition is listed in Table 1.

Table 1. Composition of Xm-19

C	Si	Mn	Cr	Ni	Mo	Nb	N	Fe
≤ 0.06	≤ 0.75	4.0~ 6.0	20.5~ 23.5	11.5~ 13.5	1.5~ 3.0	0.1~ 0.3	0.2~ 0.4	Balance

Three XM-19 microstructures with different grain sizes were prepared to examine the grain-size effect on oxidation behavior. The XM-19 specimens were categorized as fine-, medium-, and coarse-grained conditions (denoted as SG, LG, and XL, respectively). The average grain sizes of XM-19 (SG/LG/XL) and 304 stainless steel, measured prior to oxidation, were 40.8μm, 154.3μm, and 265.5μm for XM-19 and 29.1μm for 304, respectively. All oxidation tests and post-test characterizations were performed on these grain-size-classified specimens under identical thermal and environmental conditions.

High-temperature oxidation experiments were performed using a laboratory-built induction-heating thermogravimetric setup; a schematic of the apparatus is provided in Fig. 1. The specimen was suspended from the lower hook of a microbalance and placed inside a glass tube to continuously record mass change in real time during exposure. Heating was provided using an induction coil, while the specimen temperature was monitored using a non-contact infrared thermometer (pyrometer). Oxidation tests were conducted at 800, 900, 1000, and 1100℃, and each condition was maintained isothermally for 2 h.

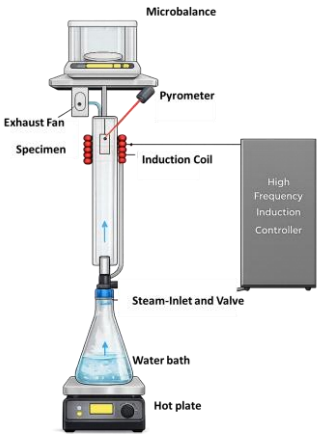

Fig. 1. Schematic diagram of the experiment

Two environmental conditions were investigated: (i) ambient laboratory air and (ii) a steam-rich open configuration. For the steam environment, water was heated in a flask placed on a hotplate to generate steam, which was introduced into the reaction tube through an inlet. The steam flowed past the heated specimen and was exhausted through the open outlet at the top of the tube; a fan was used to promote stable upward flow and to minimize condensation effects near the balance For the air condition, the specimen was heated under identical thermal conditions without intentional introduction of water vapor.

The phase constitution of oxide scales was analyzed by X-ray diffraction (XRD) using Cu-Kα radiation. Surface morphology and oxide-scale chemistry were examined using scanning electron microscopy (SEM) equipped with energy-dispersive X-ray spectroscopy (EDS). Cross-sectional specimens were prepared to measure oxide-scale thickness and to assess the elemental distribution as a function of depth.

3. Results and Discussion

Fig. 2 shows the temperature-dependent mass gain of the specimens oxidized in air. At 800℃ and 900℃, the mass gain was comparable among the specimens, suggesting that differences in oxidation behavior were not pronounced in this temperature range. As the temperature increased to 1000℃ and 1100℃, however, the differences became clearer. The largest variation was observed at 1100℃, where XM-19 exhibited an apparent grain-size dependence, with larger-grained specimens showing higher mass gain. In addition, comparison with 304 stainless steel indicates that 304 experienced higher mass gain than XM-19 under the same conditions. Overall, these results suggest that XM-19 shows better oxidation resistance in air at elevated temperatures, and that microstructural factors such as grain size can affect oxidation kinetics more strongly at higher temperatures.

Fig. 3 illustrates the mass gain of specimens oxidized in steam. At both 1000℃ and 1100℃, the 304 specimen exhibited substantially higher mass gain than XM-19 (SG/LG/XL). In particular, the increase in mass gain from 1000 ℃ to 1100 ℃ was much larger for 304, consistent with accelerated oxidation at the higher temperature. XM-19 also showed a grain-size dependence, with mass gain increasing as grain size increased.

Compared with the air results, the overall mass gain in steam was markedly higher, confirming that steam provides a more aggressive environment for high-temperature oxidation [1]. This behavior is consistent with the notion that water vapor can accelerate oxide growth and increase the likelihood of protective-scale degradation (e.g., cracking/spallation), which in turn can lead to higher net mass gain. The observed increase in mass gain with increasing grain size in XM-19 may be associated with microstructural effects on the establishment and maintenance of a Cr-rich protective scale. For example, a reduced grain boundary density in coarse-grained specimens can decrease fast diffusion pathways and may retard the effective supply of Cr to the surface, thereby delaying the development of a continuous Cr-rich inner layer [2]. In addition, the consistently higher mass gain of 304 relative to XM-19 under identical conditions likely reflects differences in alloy chemistry and scale stability, including the ability to form and sustain Cr-rich protective layers. Together, the results indicate that XM-19 has comparatively superior oxidation resistance in high-temperature steam within the conditions examined.

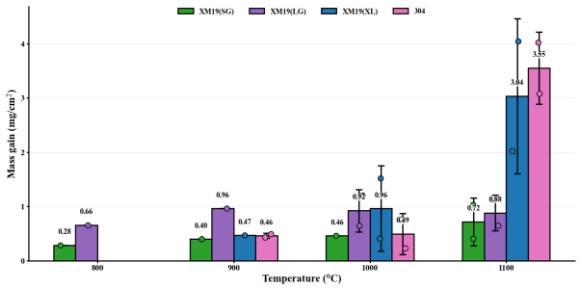

Fig. 2. Oxidation of Xm-19 and 304 at 800℃, 900℃, 1000℃ and 1100℃ in air

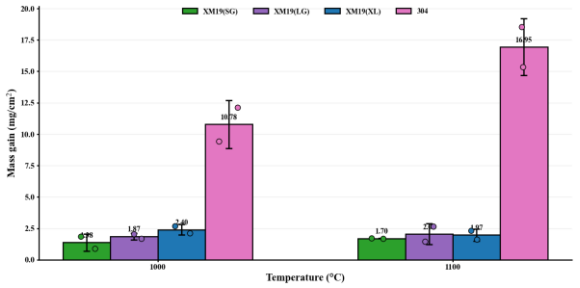

Fig. 3. Oxidation of Xm-19 and 304 at 1000℃ and 1100℃ in steam

Fig. 4 presents oxide-scale thickness measurements from cross-sectional specimens after oxidation in steam. At 1000℃, the differences in oxide thickness among XM-19 grain sizes (SG, LG, and XL) were relatively small and not readily distinguishable. In contrast, at 1100℃ a more pronounced grain-size dependence was

observed, with measurable differences in oxide thickness among the specimens. These results indicate that microstructural factors, such as grain size, can have a stronger influence on oxide growth at higher temperatures [2].

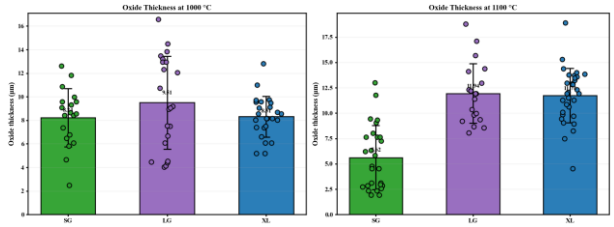

Fig. 4. Oxide scale thickness measured after oxidation in steam at 1000℃ and 1100℃

Fig. 5 shows surface morphologies after oxidation in air. At 800℃, no clear evidence of large-scale spallation was observed. As the temperature increased to 900℃, 1000℃, and 1100℃, surface damage consistent with spallation became more apparent, suggesting reduced scale adherence/stability at elevated temperatures.

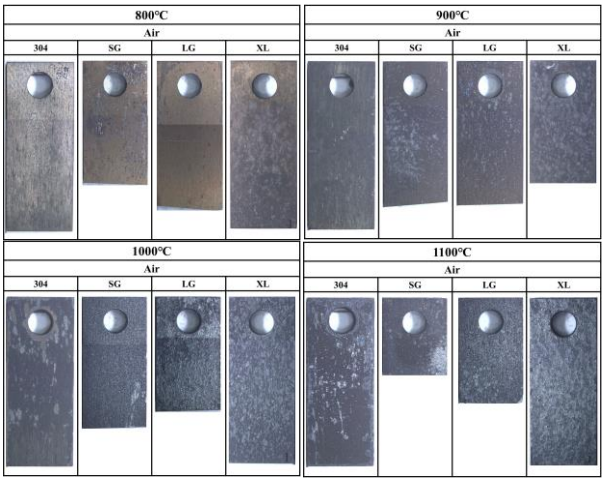

Fig. 5 Surface appearance of 304 and XM-19 specimens with different grain sizes (SG, LG and XL) after oxidation at 800℃~1100℃ in air

Fig. 6 shows surface morphologies after oxidation in steam. Compared with air, spallation-like surface damage occurred more readily in steam, consistent with the higher mass gain and thicker scales formed under steam exposure. At 1100℃, the 304 specimen showed more extensive spallation than XM-19. These observations support that steam accelerates oxidation and can promote scale degradation (cracking/spallation), especially at higher temperatures.

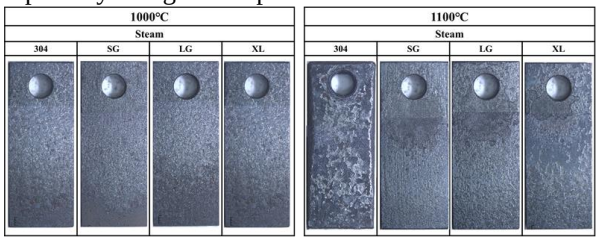

Fig. 6 Surface appearance of 304 and XM-19 specimens with different grain sizes (SG, LG and XL) after oxidation at 1000℃ and 1100℃ in steam

Fig. 7 presents representative cross-sectional SEM images and EDS elemental maps of specimens oxidized in steam, arranged in the order of XL, LG, and SG grain sizes. A duplex oxide structure was observed after steam exposure. Oxygen was detected throughout the oxide scale, consistent with the formation of a continuous oxide layer. Chromium was enriched near the oxide/metal interface, indicating a Cr-rich inner region, whereas iron was concentrated toward the outer region, indicating the development of an Fe-rich outer layer. This duplex architecture—an inner Cr-rich layer coupled with an outer Fe-rich oxide—has been widely reported for austenitic stainless steels under steam-containing environments.

Manganese showed a distribution trend broadly similar to iron, which is consistent with the possible formation of Mn-containing spinel-type oxides within the outer region. Manganese exhibited a distribution pattern similar to that of iron, suggesting the formation of Mn-containing spinel phases [3], such as $MnCr_2O_4$, within the outer oxide region. The compositional gradient across the scale implies outward diffusion of Fe and Mn and inward diffusion of oxygen during high-temperature steam oxidation.

At 1100℃, the oxide scale became significantly thicker and the compositional contrast more pronounced, particularly in the coarse-grained (XL) specimen. This trend weakened as the grain size decreased from LG to SG. The enhanced oxidation in coarse-grained XM-19 is consistent with the interpretation that reduced grain boundary density may limit Cr transport to the growing scale and delay the establishment of a stable, continuous Cr-rich protective layer, as reported in previous studies on grain-size effects in stainless steels [2,4].

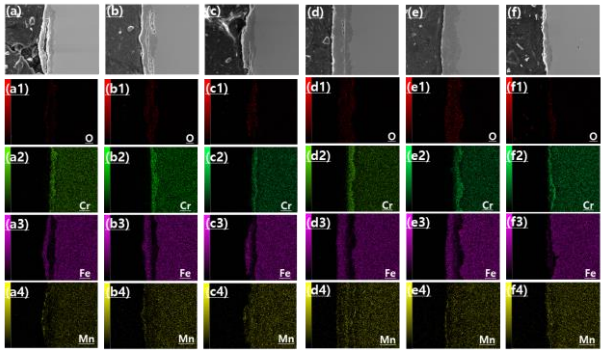

Fig. 7 Cross-sectional SEM/EDS maps of XM-19 oxidized in steam: 1000℃ (a–c: XL, LG, SG) and 1100℃ (d–f: XL, LG, SG)

Fig. 8 presents the XRD patterns obtained to identify the phase evolution of oxide products under different oxidation atmospheres. Pattern (a) corresponds to specimens oxidized in air, whereas pattern (b) represents those oxidized in steam. In both conditions, diffraction peaks originating from the γ-austenitic

matrix were observed along with additional peaks attributable to oxide phases. However, noticeable differences in relative peak intensities and phase assemblages were identified depending on the oxidation environment.

Under air oxidation, conditions favorable for the formation of protective oxides resulted in relatively pronounced Cr-based oxide peaks (e.g., Cr_2O_3) or Cr-containing oxide phases. In contrast, steam oxidation promoted the formation of Fe-based oxides (e.g., Fe_3O_4 and/or Fe_2O_3), as evidenced by the increased intensity of corresponding diffraction peaks. In addition, spinel-type oxides containing manganese, such as $MnCr_2O_4$ and Fe_2MnO_4, were detected under the steam condition. The formation and thermodynamic stability of Mn–Cr–O spinel phases (e.g., $MnCr_2O_4$) at high temperatures have been previously reported [5], supporting the phase identification in the present study. These results are consistent with the EDS observations in Fig. 7, which revealed manganese enrichment in the outer oxide region together with iron, suggesting the participation of Mn in spinel-type oxide formation.

Overall, the XRD results corroborate the duplex oxide structure inferred from cross-sectional EDS analysis, consisting of a Cr-rich inner layer and an Fe-rich outer layer under steam oxidation. The increased contribution of Fe-based oxides and Mn-containing spinel phases (Fe_2MnO_4, $MnCr_2O_4$) under the steam environment indicates enhanced outer-scale growth and compositional evolution under high-temperature steam conditions.

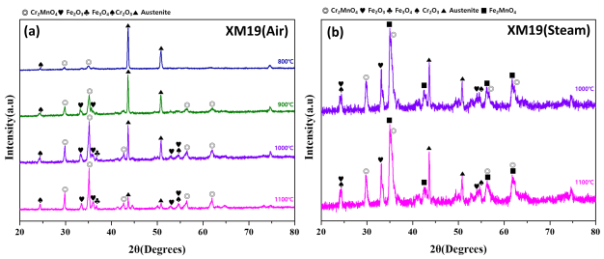

Fig. 8 XRD patterns of the oxidized specimens: (a) oxidation in air and (b) oxidation in steam

4. Conclusion

In this study, the high-temperature oxidation behavior of XM-19 was systematically compared with that of type 304 stainless steel in air and steam environments at 800–1100℃, with particular emphasis on grain-size effects.

Oxidation in steam resulted in substantially higher mass gain and more pronounced spallation-like surface damage than oxidation in air, confirming the more aggressive nature of steam-containing environments under the conditions examined. Under both atmospheres, type 304 exhibited higher mass gain and thicker oxide scales than XM-19, indicating comparatively poorer oxidation resistance.

A grain-size dependence was observed in XM-19 at elevated temperatures (1000–1100℃), where coarse-grained specimens showed increased mass gain and oxide thickness. This trend is consistent with microstructural effects on the establishment of Cr-rich protective layers; in coarse-grained materials, the reduced grain boundary density may decrease fast diffusion pathways and retard the effective supply of chromium to the growing scale, thereby delaying the development of a continuous protective inner layer.

Overall, XM-19 demonstrated better high-temperature oxidation resistance than type 304, particularly under steam exposure. These findings support the potential of XM-19 as a candidate material for structural components in advanced nuclear systems, including SMRs, where high-temperature steam environments may be encountered.

REFERENCES

[1] J. T. Bittel, L. H. Sjodahl, J. F. White; Oxidation of 304L Stainless Steel by Steam and by Air*. *CORROSION* 1 January 1969; 25 (1): 7–14.

[2] Kim, J. H., Kim, D. I., Suwas, S., Fleury, E., Yi, K. W.; Grain-size effects on the oxidation of modified 304 austenitic stainless steel. Oxidation of Metals April 2013; 79 (3-4): 239–247.

[3] Hao Li, Weixing Chen; High temperature carburization behaviour of Mn–Cr–O spinel oxides with varied concentrations of manganese. *Corrosion Science* 1 June 2011; 53 (6): 2097–2105.

[4] Liang, Z., Zhao, Q.; Steam Oxidation of Austenitic Heat-Resistant Steels TP347H and TP347HFG at 650–800 ℃. Materials (Basel) 14 February 2019; 12 (4): 577.

[5] Li, H., Chen, W.; High temperature carburization behaviour of Mn–Cr–O spinel oxides with varied concentrations of manganese. Corrosion Science 1 June 2011; 53(6): 2097–2105